Coherent exciton-phonon coupling in perovskite semiconductor nanocrystals studied by two-dimensional electronic spectroscopy

Wei Zhao, Zhengyuan Qin, Chunfeng Zhang 🆔, Guodong Wang, Xingcan Dai, and Min Xiao

View Online   Export Citation   CrossMark

ARTICLES YOU MAY BE INTERESTED IN

Coherent exciton-phonon coupling in perovskite semiconductor nanocrystals studied by two-dimensional electronic spectroscopy

Wei Zhao,[1,2] Zhengyuan Qin,[2] Chunfeng Zhang,[2,a] [ID] Guodong Wang,[2] Xingcan Dai,[1,b] and Min Xiao[2,3,c]

AFFILIATIONS

[1]Department of Physics, Tsinghua University, Beijing 100084, China
[2]National Laboratory of Solid State Microstructures, School of Physics, and Collaborative Innovation Center of Advanced Microstructures, Nanjing University, Nanjing 210093, China
[3]Department of Physics, University of Arkansas, Fayetteville, Arkansas 72701, USA

[a]E-mail: cfzhang@nju.edu.cn
[b]E-mail: xingcandai@mail.tsinghua.edu.cn
[c]E-mail: mxiao@uark.edu

ABSTRACT

Perovskite semiconductor nanocrystals of lead halides exhibit excellent electronic and optical properties that are suitable for many optoelectronic applications. In this report, we investigate the underlying mechanism of the optical response of the material by probing coherent interaction between the exciton and lattice vibration by two-dimensional electronic spectroscopy. Coherent exciton-phonon coupling has been observed with time-domain oscillations in the dynamics of signals related to either ground or excited electronic states. Furthermore, the spectra of the coherent phonon derived from the dynamics of biexciton formation have larger amplitudes for higher frequency modes, which is attributed to the phonon bottleneck effect. Moreover, the composition-dependent coherent coupling between the exciton and lattice vibration in mixed halide samples reveals a critical role played by the anharmonicity and fluctuation of lattice vibration in the excited-state dynamics of perovskite nanocrystals.

Published under license by AIP Publishing. https://doi.org/10.1063/1.5130636

Lead halide perovskites have emerged as an excellent family of semiconductors for solar conversion and light-emitting devices[1–4] due to their long carrier lifetimes, long carrier diffusion lengths, and exceptional defect tolerance.[5–10] A large number of studies exploring the underlying mechanism suggest that the carrier-phonon coupling is responsible for the optoelectronic response in perovskite semiconductors that share a common $APbX_3$ structure (A = methylammonium, formamidinium, or Cs; X = Cl, Br, or I). The crystal structure consists of a sublattice of corner-sharing PbX_6^{3-} octahedra and a sublattice of A^+ cations in the cubic octahedral voids, leading to intrinsic softness and dynamic disorder.[11,12] The coupling between the carrier and lattice vibration in lead halide films has been studied by Raman, infrared, and photoluminescence (PL) spectroscopies,[13–24] as well as time-resolved spectroscopy.[6,25,26] It was proposed that the scattering between charge carriers and defects is reduced by large polarons with screening Coulomb potential formed by electron-phonon coupling in lead halides. In such a scenario, the correlated coherent motion of

charge carriers and polar lattice is essential for the enhanced carrier lifetimes in the perovskite semiconductors.

Recently, light emitting performance of lead halide perovskite materials has been further optimized by employing quantum confinement effects in nanocrystal structures, leading to remarkable progress in light-emitting diodes,[27–30] lasers,[31,32] and quantum emitters.[33–35] In particular, the bandgap of semiconductor nanocrystals can be continuously detuned by mixing the halide element through simple anion exchange procedures.[36] In strongly confined nanocrystals of lead halides, exciton-phonon coupling plays a pivotal role in the quantum dephasing dynamics of excitons, as manifested with linewidth broadening and fine structures in the emission spectra of single nanocrystals.[35,37] The strong Fröhlich electron-phonon interaction slows down the relaxation of hot carriers, known as the phonon bottleneck effect in perovskite nanocrystals.[38–40] However, there are a limited number of studies on the lattice dynamics of perovskite nanocrystals. Raman

spectroscopy has identified multiple vibrational modes that are coupled to the ground electronic state.[41,42] It remains poorly understood how the vibration of lattices affects the excited electronic states in perovskite nanocrystals.

In this work, we study the coherent exciton-lattice vibration interaction in perovskite $CsPbX_3$ nanocrystals (NCs) by using two-dimensional electronic spectroscopy (2DES).[43,44] Vibrational coherence at room temperature is observed in the 2DES signal with oscillations in the time domain in the modes of the Pb-X-Pb bending and Pb-X stretching. Furthermore, by analyzing the contributions from different Feynman pathways, vibrational coherence from ground- and excited-electronic states can be separated, suggesting a critical role played by carrier-lattice interaction to the excited state dynamics in perovskite nanocrystals. In comparison with the coherent phonon spectrum at the dynamics of photoinduced bleaching, the spectral features of coherent phonons at the biexciton formation dynamics have greater amplitude in higher frequency modes, which is a signature of the phonon bottleneck effect. Moreover, the different halide composition-dependent dynamics of fundamental and second-order Pb-X stretching modes suggest exotic optoelectronic properties related to the anharmonic and disordered lattice vibration due to phase segregation in anion-exchanged lead halide perovskite nanocrystals.

The samples are synthesized by hot-injection with a bandgap tunable through an anion-exchange reaction.[36] Figure 1(a) presents the absorption and photoluminescence spectra of a toluene solution sample of $CsPbBr_3$ nanocrystals in cubic shapes with an average length of 10 nm. The Raman spectrum of a NC film ($>80\,cm^{-1}$) shown in Fig. 1(b) exhibits multiple scattering peaks with Lorentz function profiles. According to the previous studies,[14,21,45] we assign the peak around $53\,cm^{-1}$ to the Pb-Br-Pb bending mode and the peaks at 127 and $155\,cm^{-1}$ to the longitudinal optical (LO) phonon modes related to the Pb-Br stretching of the PbX_3^- sublattice. The broad peak at $310\,cm^{-1}$ appears as a high-order scattering mode.

We conduct 2DES measurements on the solution sample of $CsPbBr_3$ NCs at different population delays (T). Figure 2(a) shows a slice of the absorptive 2D electronic spectrum at $T = 250\,fs$. The peak located upon the diagonal line is due to the photoinduced bleaching (PIB), and the negative signals above and under PIB are the features of excited state absorption (labeled as ESA_1 and ESA_2). The coherent electron-phonon coupling is manifested as oscillations in the time domain dynamics.[46,47] We extract the oscillatory components from the time traces of the three featured peaks [Fig. 2(b)] by subtracting the exponential decay components. Figures 2(c) and 2(d) show the oscillations in the time domain and the spectra in the frequency domain obtained by Fourier transformation. While the oscillation frequencies resonate to the Pb-Br stretching phonon modes in $CsPbBr_3$ NCs of 155 and $310\,cm^{-1}$ (denoted as LO_1 and LO_2 modes in the following), a low-frequency mode at $\sim50\,cm^{-1}$ related to the Pb-Br-Pb bending mode is also observed. The oscillations observed in the traces of both PIB and ESA signals suggest the possible coupling between ground/excited electronic states and coherent lattice vibrations.

The coupling of lattice vibration to the excited or the ground electronic states may play significantly different roles in determining the optoelectronic response, which has been intensively studied in various light harvesting systems.[26,48] To elucidate the origins of coherent electron-phonon coupling for the ground and the excited electronic
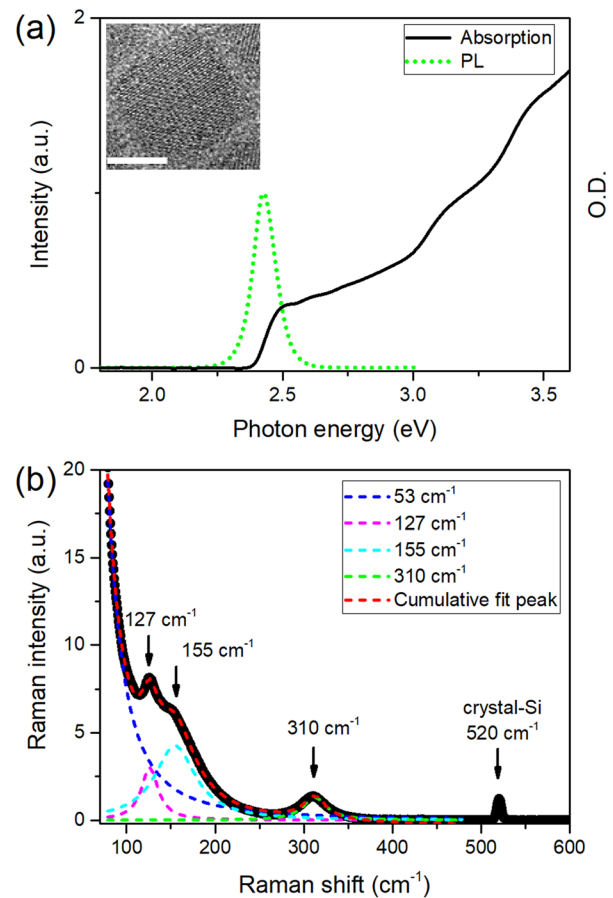

FIG. 1. (a) Absorption (solid) and normalized PL (dot) spectra of a solution sample of $CsPbBr_3$ NCs. The inset shows a typical transmission electron microscopy (TEM) image of a nanocrystal (scale bar: 5 nm). (b) A Raman spectrum (black dot) of a $CsPbBr_3$ NC film dropped on a crystal silicon substrate. The spectrum in the range of 80–$480\,cm^{-1}$ can be reproduced with four peaks of Lorentz function profiles.

states, relevant Liouville-space pathways are illustrated by double-sided Feynman diagrams as shown in Fig. 2(e). Consistent with the theoretical prediction [Fig. 2(e)], the oscillations at the ESAs exhibit a π-phase shift in the phase from those at the PIB contributed by the processes of ground state bleaching (GSB) and stimulated emission (SE) [Fig. 2(c)]. Therefore, the oscillations retrieved from the ESA dynamics are caused by coherent lattice vibration coupled with excited electronic states. Notably, different patterns have been observed at the time domain dynamics of ESA_1 and ESA_2 signals, which is plausibly related to different electronic transitions involved. The oscillation amplitude in the dynamics of ESA_1 is relatively weaker than that in the PIB [Fig. 2(c)], but their frequency profiles are still similar [Fig. 2(d)]. This suggests that ESA_1 is the transition from long-lived low-lying excitons to higher excited states. In contrast, the oscillation amplitude is more pronounced for higher energy vibration modes in the dynamics of ESA_2 [Fig. 2(d)]. ESA_2 has been assigned to the short-lived process of biexciton formation.[49] The greater amplitude for the higher frequency mode is plausibly caused by the phonon bottleneck effect during the biexciton
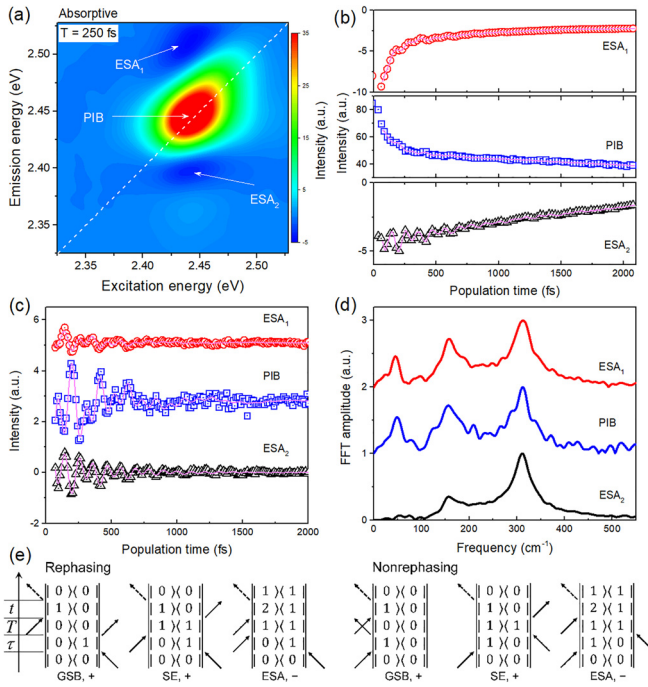
FIG. 2. (a) Absorptive 2DES spectrum of CsPbBr$_3$ NCs at $T = 250$ fs. The features of PIB and two ESAs are marked by arrows. (b) The temporal dynamics of signals probed at the PIB and two ESA features. (c) The oscillation components obtained by subtracting the exponential decay components in (b). (d) Normalized Fourier transform spectra of the oscillations for the PIB and two ESA features. (e) Double sided Feynman diagrams of rephasing and nonrephasing pathways; their corresponding signals generate the absorptive 2DES. $|0\rangle$, $|1\rangle$, and $|2\rangle$ denote the ground, low-lying, and higher excited states, respectively. The sign $[(-1)^n]$ of a diagram is determined by the number (n) of the interactions (arrows) on the right side. The different signs result in a phase difference of π between the oscillations upon PIB (GSB and SE) and ESA.

FIG. 3. (a) The real part of the rephasing 2DES spectrum of the solution sample of CsPbBr$_3$ NCs at $T = 250$ fs. The position of the PIB is marked by a black square. (b) The PIB oscillation components are extracted from complex rephasing 2DES dynamics. (c) The Feynman diagrams elucidate the oscillating components concealed in PIB. The oscillations of SE and GSB correspond to negative and positive frequencies (ω_T), respectively. (d) The normalized Fourier transform spectrum of complex oscillation upon PIB. The half part with negative frequency contains the coupling from excited states (SE), while the positive part contains couplings from the ground state (GSB).

FIG. 4. The beating maps generated from the complex signal of rephasing 2DES measurements of CsPbBr$_3$ NC solution. These four maps represent the oscillating amplitude distributions corresponding to different frequencies (±155 and ±310 cm^{-1}), respectively. The marks indicate the signal coordinates predicted by double-sided Feynman diagrams, while the circle and down and up triangles mean GSB and SE and ESA. Roman numerals relate each mark to a specific Liouville-space pathway demonstrated in Figs. S2–S4 in the supplementary material.

formation where the higher energy mode of lattice vibration is more efficient for compensating the biexciton binding energy.

For the signal of the PIB [Figs. 2(a) and 3(a)], contributions from both the ground electronic state (GSB) and excited electronic states through the SE process are involved. Due to the spectral overlap, the oscillations tagged on the ground and excited electronic states for vibrational coherence are always entangled, which is challenging for the coupling to be distinguished by conventional experimental approaches. Here, we analyze the complex oscillating dynamics [Fig. 3(b)] by Fourier transformation, where the coherent behaviors related to the GSB and SE processes can be described by the Liouville-space pathways for the rephasing 2D signal [Fig. 3(c)]. In our discussion below, ground, low-lying excited, and double excited electronic states are indicated by $|0\rangle$, $|1\rangle$, and $|2\rangle$, and a state coupled with the phonon is designated as the state number n with a single quotation mark ($|n'\rangle$). If coherence persists for much longer than the laser pulse duration during the population decay processes, the oscillation component of the 2DES signal is detectable in the T domain. Furthermore, the signals corresponding to $|0'\rangle\langle0|$ or $|1'\rangle\langle1|$ oscillate with negative frequencies ($\omega_T < 0$), while those of $|0\rangle\langle0'|$ and $|1\rangle\langle1'|$ are detectable in the positive range in the x axis ($\omega_T > 0$).[46,47] We list all rephasing
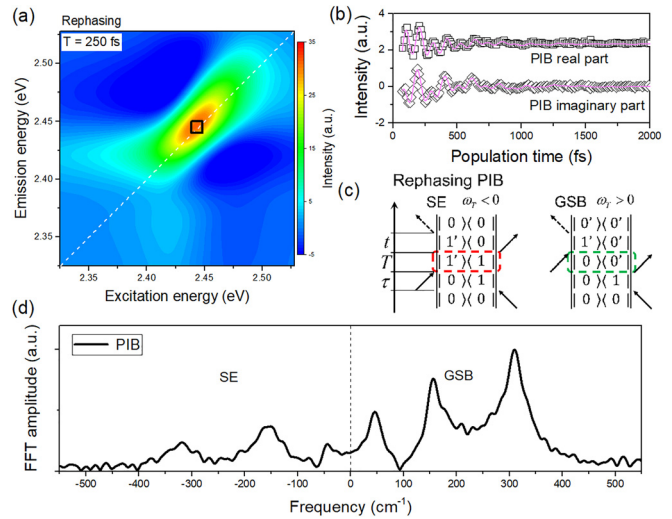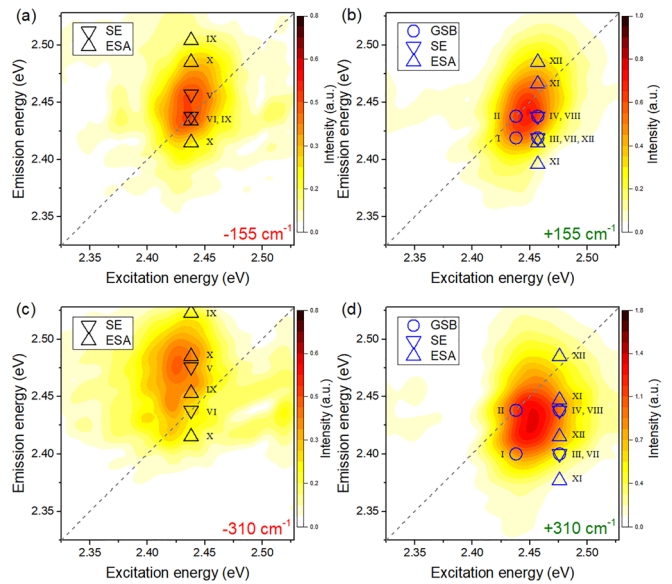
diagrams containing the vibrational coupling in the three types of pathways, GSB, SE, and ESA [Figs. S2–S4 in the supplementary material]. Figure 4 shows the beating maps generated from rephasing 2DES signals, representing the oscillation amplitudes at different excitation and emission photon energies for different vibrational modes (± 155 and $\pm 310\,cm^{-1}$). The beating map is consistent with our above assessment as marked in Fig. 4 corresponding to the energy coordinate of coherent coupling oscillation predicted for varying Liouville-space pathways. These results clearly separate the vibrational coherences from ground- and excited-electronic states where coherent oscillations tagged at ground excited states are absent at negative frequency. Through this method, in the positive or negative frequency range [Fig. 3(d)], the oscillation component of the PIB signal related to the ground (GSB) or excited (SE) electronic states can be distinguished, where the modes of Pb-X stretching strongly modulate the SE dynamics.

The spectral profiles of multiple modes observed in the dynamics tagged ground and excited electronic states are asymmetric and broad, implying the anharmonicity and dynamic disorder of lattice vibrations. To gain more insights into the coherent carrier-phonon interaction, we study the $CsPbX_3$ nanocrystals with different halide ratios between Br and I (Fig. S1). Similar oscillations can be detected from the PIB signals of different samples [Figs. 5(a) and 5(b)]. As shown in
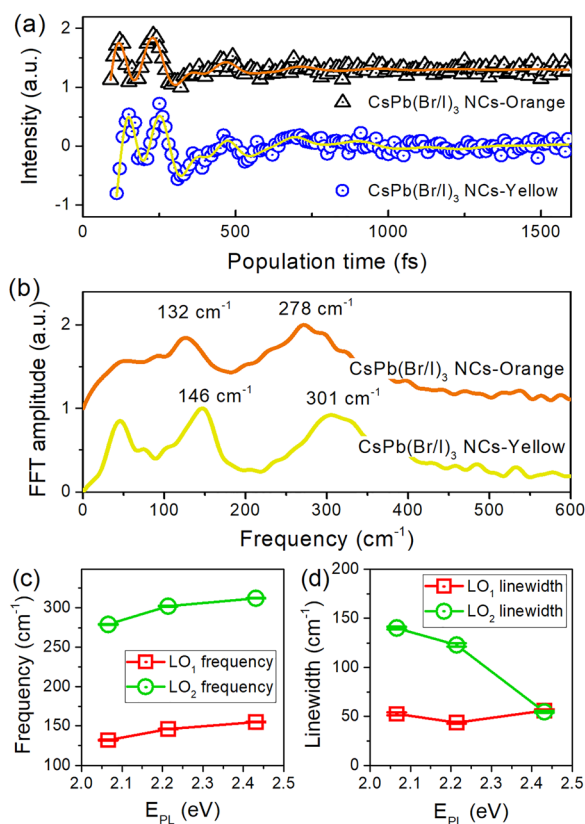
Fig. 5(c), when the compositional ratio of iodine ions increases, the frequencies of phonon modes decrease. This phonon softening behavior further confirms that these phonon modes are induced by lattice vibrations of the PbX_6^{3-} octahedral sublattice in perovskite nanocrystals.

The coherent phonons in the mixed halide nanocrystals show some difference from that in the $CsPbBr_3$ nanocrystals with pure halide. In the phonon spectra of the mixed halide nanocrystals, the frequency of the LO_2 phonon is slightly different from twice of the frequency of the LO_1 phonon [Fig. 5(c)]. In addition, the spectra of characteristic phonon modes are much broader, suggesting a faster decoherence of the lattice vibrations in the mixed halide samples [Fig. 5(d)]. Such differences can be explained due to the inhomogeneity of mixed halide samples. In the aqueous samples, the halide element exchanges with that in the solution and the ion migration effect possibly causes the dynamic fluctuation of the composition and structure, leading to additional anharmonicity and spectral broadening. The sublattice anharmonicity and dynamic disorder are the typical characteristics of large polaron formation in bulk lead halide perovskites,[11,45] implying the possibility of manipulating the dynamics of charge carriers through composition engineering.

In summary, coherent interactions between excitons and lattice vibrations in $CsPbX_3$ nanocrystals in solution have been studied by 2DES measurements. By analyzing different pathways of electronic transitions, we can isolate the features of vibrational coherence involved in the transitions related to the excited electronic states. The phonon bottleneck effect is also observed during the biexciton formation, which results in greater amplitude for the higher frequency vibration modes in the spectra of coherent phonons. These findings suggest that the optoelectronic properties of perovskite nanocrystals may be further optimized by manipulating the interplay between the electronic and lattice degrees of freedom.

See the supplementary material for the optical characterization and sample preparation details, absorption and PL spectra of samples (Fig. S1), Feynman diagrams of rephasing 2DES signals (Figs. S2–S4), absorptive 2DES spectra, and PIB dynamic evolutions of anion-exchanged $CsPb(Br/I)_3$ NCs (Fig. S5).

FIG. 5. (a) The oscillations in the dynamics of the PIB signal extracted from the absorptive 2DES of yellow and orange-emitting $CsPb(Br/I)_3$ NCs. (b) The FFT spectra of oscillations in (a) for the two $CsPb(Br/I)_3$ NC samples. (c) and (d) The frequencies and linewidths of the two oscillation modes in the samples with different PL photon energies.

REFERENCES

[1]W. Zhang, G. E. Eperon, and H. J. Snaith, Nat. Energy **1**, 16048 (2016).

[2]T. Leijtens, K. A. Bush, R. Prasanna, and M. D. McGehee, Nat. Energy **3**, 828 (2018).

[3]S. A. Veldhuis, P. P. Boix, N. Yantara, M. Li, T. C. Sum, N. Mathews, and S. G. Mhaisalkar, Adv. Mater. **28**, 6804 (2016).

[4]B. R. Sutherland and E. H. Sargent, Nat. Photonics **10**, 295 (2016).

[5]G. Xing, N. Mathews, S. Sun, S. S. Lim, Y. M. Lam, M. Grätzel, S. Mhaisalkar, and T. C. Sum, Science **342**, 344 (2013).

[6]D. M. Monahan, L. Guo, J. Lin, L. Dou, P. Yang, and G. R. Fleming, J. Phys. Chem. Lett. **8**, 3211 (2017).

[7]Q. Dong, Y. Fang, Y. Shao, P. Mulligan, J. Qiu, L. Cao, and J. Huang, Science **347**, 967 (2015).

[8]D. Shi, V. Adinolfi, R. Comin, M. Yuan, E. Alarousu, A. Buin, Y. Chen, S. Hoogland, A. Rothenberger, K. Katsiev, Y. Losovyj, X. Zhang, P. A. Dowben, O. F. Mohammed, E. H. Sargent, and O. M. Bakr, Science **347**, 519 (2015).

[9]R. E. Brandt, J. R. Poindexter, P. Gorai, R. C. Kurchin, R. L. Z. Hoye, L. Nienhaus, M. W. B. Wilson, J. A. Polizzotti, R. Sereika, R. Žaltauskas, L. C. Lee, J. L. MacManus-Driscoll, M. Bawendi, V. Stevanović, and T. Buonassisi, Chem. Mater. **29**, 4667 (2017).

[10]R. E. Brandt, V. Stevanović, D. S. Ginley, and T. Buonassisi, MRS Commun. **5**, 265 (2015).

[11]K. Miyata, T. L. Atallah, and X. Y. Zhu, Sci. Adv. **3**, e1701469 (2017).

[12]F. Bertolotti, L. Protesescu, M. V. Kovalenko, S. Yakunin, A. Cervellino, S. J. L. Billinge, M. W. Terban, J. S. Pedersen, N. Masciocchi, and A. Guagliardi, ACS Nano **11**, 3819 (2017).

[13]C. Carabatos-Nédelec, M. Oussaïd, and K. Nitsch, J. Raman Spectrosc. **34**, 388 (2003).

[14]C. Quarti, G. Grancini, E. Mosconi, P. Bruno, J. M. Ball, M. M. Lee, H. J. Snaith, A. Petrozza, and F. De Angelis, J. Phys. Chem. Lett. **5**, 279 (2014).

[15]M. Ledinský, P. Löper, B. Niesen, J. Holovský, S.-J. Moon, J.-H. Yum, S. De Wolf, A. Fejfar, and C. Ballif, J. Phys. Chem. Lett. **6**, 401 (2015).

[16]F. Brivio, J. M. Frost, J. M. Skelton, A. J. Jackson, O. J. Weber, M. T. Weller, A. R. Goñi, A. M. A. Leguy, P. R. F. Barnes, and A. Walsh, Phys. Rev. B **92**, 144308 (2015).

[17]J. Tilchin, D. N. Dirin, G. I. Maikov, A. Sashchiuk, M. V. Kovalenko, and E. Lifshitz, ACS Nano **10**, 6363 (2016).

[18]K.-H. Wang, L.-C. Li, M. Shellaiah, and K. Wen Sun, Sci. Rep. **7**, 13643 (2017).

[19]M. A. Pérez-Osorio, R. L. Milot, M. R. Filip, J. B. Patel, L. M. Herz, M. B. Johnston, and F. Giustino, J. Phys. Chem. C **119**, 25703 (2015).

[20]B.-W. Park, S. M. Jain, X. Zhang, A. Hagfeldt, G. Boschloo, and T. Edvinsson, ACS Nano **9**, 2088 (2015).

[21]J.-H. Cha, J. H. Han, W. Yin, C. Park, Y. Park, T. K. Ahn, J. H. Cho, and D.-Y. Jung, J. Phys. Chem. Lett. **8**, 565 (2017).

[22]O. Yaffe, Y. Guo, L. Z. Tan, D. A. Egger, T. Hull, C. C. Stoumpos, F. Zheng, T. F. Heinz, L. Kronik, M. G. Kanatzidis, J. S. Owen, A. M. Rappe, M. A. Pimenta, and L. E. Brus, Phys. Rev. Lett. **118**, 136001 (2017).

[23]M. Sebastian, J. A. Peters, C. C. Stoumpos, J. Im, S. S. Kostina, Z. Liu, M. G. Kanatzidis, A. J. Freeman, and B. W. Wessels, Phys. Rev. B **92**, 235210 (2015).

[24]A. D. Wright, C. Verdi, R. L. Milot, G. E. Eperon, M. A. Pérez-Osorio, H. J. Snaith, F. Giustino, M. B. Johnston, and L. M. Herz, Nat. Commun. **7**, 11755 (2016).

[25]G. Batignani, G. Fumero, A. R. Srimath Kandada, G. Cerullo, M. Gandini, C. Ferrante, A. Petrozza, and T. Scopigno, Nat. Commun. **9**, 1971 (2018).

[26]F. Thouin, D. A. Valverde-Chávez, C. Quarti, D. Cortecchia, I. Bargigia, D. Beljonne, A. Petrozza, C. Silva, and A. R. Srimath Kandada, Nat. Mater. **18**, 349 (2019).

[27]S. Adjokatse, H.-H. Fang, and M. A. Loi, Mater. Today **20**, 413 (2017).

[28]L. Protesescu, S. Yakunin, M. I. Bodnarchuk, F. Krieg, R. Caputo, C. H. Hendon, R. X. Yang, A. Walsh, and M. V. Kovalenko, Nano Lett. **15**, 3692 (2015).

[29]Z. Bai and H. Zhong, Sci. Bull. **60**, 1622 (2015).

[30]H. C. Yoon, H. Kang, S. Lee, J. H. Oh, H. Yang, and Y. R. Do, ACS Appl. Mater. Interfaces **8**, 18189 (2016).

[31]S. Yakunin, L. Protesescu, F. Krieg, M. I. Bodnarchuk, G. Nedelcu, M. Humer, G. De Luca, M. Fiebig, W. Heiss, and M. V. Kovalenko, Nat. Commun. **6**, 8056 (2015).

[32]Y. Xu, Q. Chen, C. Zhang, R. Wang, H. Wu, X. Zhang, G. Xing, W. W. Yu, X. Wang, Y. Zhang, and M. Xiao, J. Am. Chem. Soc. **138**, 3761 (2016).

[33]F. Hu, H. Zhang, C. Sun, C. Yin, B. Lv, C. Zhang, W. W. Yu, X. Wang, Y. Zhang, and M. Xiao, ACS Nano **9**, 12410 (2015).

[34]G. Rainò, G. Nedelcu, L. Protesescu, M. I. Bodnarchuk, M. V. Kovalenko, R. F. Mahrt, and T. Stöferle, ACS Nano **10**, 2485 (2016).

[35]M. Fu, P. Tamarat, J.-B. Trebbia, M. I. Bodnarchuk, M. V. Kovalenko, J. Even, and B. Lounis, Nat. Commun. **9**, 3318 (2018).

[36]G. Nedelcu, L. Protesescu, S. Yakunin, M. I. Bodnarchuk, M. J. Grotevent, and M. V. Kovalenko, Nano Lett. **15**, 5635 (2015).

[37]J. Ramade, L. M. Andriambariarijaona, V. Steinmetz, N. Goubet, L. Legrand, T. Barisien, F. Bernardot, C. Testelin, E. Lhuillier, A. Bramati, and M. Chamarro, Appl. Phys. Lett. **112**, 072104 (2018).

[38]P. Papagiorgis, L. Protesescu, M. V. Kovalenko, A. Othonos, and G. Itskos, J. Phys. Chem. C **121**, 12434 (2017).

[39]M. Li, S. Bhaumik, T. W. Goh, M. S. Kumar, N. Yantara, M. Grätzel, S. Mhaisalkar, N. Mathews, and T. C. Sum, Nat. Commun. **8**, 14350 (2017).

[40]J. Butkus, P. Vashishtha, K. Chen, J. K. Gallaher, S. K. K. Prasad, D. Z. Metin, G. Laufersky, N. Gaston, J. E. Halpert, and J. M. Hodgkiss, Chem. Mater. **29**, 3644 (2017).

[41]W. Zhou, F. Sui, G. Zhong, G. Cheng, M. Pan, C. Yang, and S. Ruan, J. Phys. Chem. Lett. **9**, 4915 (2018).

[42]M. Liao, B. Shan, and M. Li, J. Phys. Chem. Lett. **10**, 1217 (2019).

[43]R. Wang, X.-Y Huang, C.-F. Zhang, X.-Y. Wang, and M. Xiao, Chin. J. Chem. Phys. **30**, 637 (2017).

[44]A. Liu, D. B. Almeida, W.-K. Bae, L. A. Padilha, and S. T. Cundiff, J. Phys. Chem. Lett. **10**, 6144 (2019).

[45]K. Miyata, D. Meggiolaro, M. T. Trinh, P. P. Joshi, E. Mosconi, S. C. Jones, F. De Angelis, and X. Y. Zhu, Sci. Adv. **3**, e1701217 (2017).

[46]J. Seibt and T. Pullerits, J. Phys. Chem. C **117**, 18728 (2013).

[47]F. V. D. A. Camargo, L. Grimmelsmann, H. L. Anderson, S. R. Meech, and I. A. Heisler, Phys. Rev. Lett. **118**, 033001 (2017).

[48]Y. Song, C. Hellmann, N. Stingelin, and G. D. Scholes, J. Chem. Phys. **142**, 212410 (2015).

[49]W. Zhao, Z. Qin, C. Zhang, G. Wang, X. Huang, B. Li, X. Dai, and M. Xiao, J. Phys. Chem. Lett. **10**, 1251 (2019).